



# Analytic theory of complex-frequency-aided virtual absorption

IRIDANOS LOULAS,  ELENA-CHRISTINA PSYCHOGIOU, KOSMAS L. TSAKMAKIDIS,  AND NIKOLAOS STEFANOU\* 

*Section of Condensed Matter Physics, National and Kapodistrian University of Athens, University Campus, GR-157 84 Athens, Greece*

\*[nstefan@phys.uoa.gr](mailto:nstefan@phys.uoa.gr)

**Abstract:** Complex-frequency excitations have recently attracted a lot of attention owing to their ability to solve a number of extraordinary challenges in photonics, such as overcoming losses without gain in metalenses and plasmonic waveguides and achieving virtual absorption. However, the totality of the works so far has been mainly computational or experimental, and a full theory of the complex dynamics enabled by these excitations is still missing. Here, we develop a fully analytical, exact time-domain theory for the dynamical scattering of these excitations by both sides of dielectric plates, which have been used to achieve virtual absorption. Our precise theoretical analysis confirms previous observations and, in addition, reveals a number of intriguing phenomena that were previously missed, such as discontinuities in the scattering of the outgoing electromagnetic field and release of the stored energy in distinct packets.

© 2025 Optica Publishing Group under the terms of the [Optica Open Access Publishing Agreement](#)

## 1. Introduction

Complex-frequency excitations [1–3] have recently been exploited for a range of unexpected and exciting applications in photonics, from compensating losses in metamaterials and superlenses [4,5] or polaritonic propagation [6], to enabling virtual absorption [3,7–15], virtual critical coupling [16,17], virtual optical pulling forces [18], virtual parity-time symmetry [19,20], and diverse other functionalities [21–35] beyond the usual bounds on light scattering [24]. These excitations open a completely new perspective to the optical world, but the totality of studies thus far have been based on either computational or experimental techniques, as a result of which the complex dynamics enabled by these excitations are still considered peculiar and lack a full time-domain closed-form theoretical analysis.

It is the objective of the present work to introduce precisely such a theory, implemented for the general phenomenon of virtual absorption [3,7–15]. Starting from the properties of the scattering matrix  $S$  of a dielectric plate, and by performing an intricate calculation of the infinite series of the associated complex residues for complex-frequency incident fields, we manage to obtain an exact, time-domain solution for the outgoing (scattered) field based directly on the properties of the plate only, that is, on its electric permittivity, magnetic permeability and thickness. Our exact analysis fully reproduces all relevant previous computational results, but in addition sheds light on completely unexpected – and first-time introduced – phenomena that were missed by previous studies, such as discontinuous (in time) waveform of the scattered electromagnetic field and release of energy in discrete (with time) wavepackets, never before, to our knowledge, observed in wave physics and uniquely tied to the present complex-frequency time-domain problem.

## 2. Scattering matrix of a dielectric plate

In this work, we focus on a lossless, homogeneous, and isotropic plate of thickness  $L$ , characterized by constant relative electric permittivity  $\epsilon_2$  and magnetic permeability  $\mu_2$ , which was the simple structure used in the original work that first demonstrated the phenomenon of coherent virtual

absorption [3,8]. The plate is embedded in an otherwise homogeneous, isotropic, and lossless medium, with constant relative permittivity  $\epsilon_1$  and permeability  $\mu_1$ . The corresponding refractive indices and wave impedances are  $n_2 = \sqrt{\epsilon_2\mu_2}$ ,  $Z_2 = \sqrt{\mu_2/\epsilon_2}$  for the plate, and  $n_1 = \sqrt{\epsilon_1\mu_1}$ ,  $Z_1 = \sqrt{\mu_1/\epsilon_1}$  for the surrounding medium. We further assume that the plate is perpendicular to the  $x$ -axis, which is directed from left to right, as presented in Fig. 1. It is worth noting that, since throughout this paper we consider the electric permittivity and magnetic permeability of both the plate and the surrounding medium to be constant (i.e., frequency-independent), the findings remain applicable across different frequency and time ranges, provided that the plate thickness is scaled accordingly.

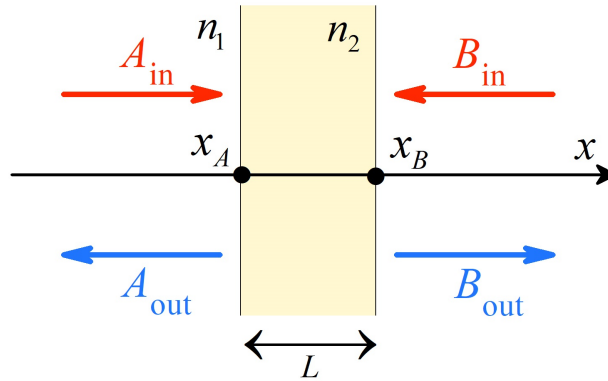


**Fig. 1.** Schematic representation of electromagnetic wave scattering by a plate of thickness  $L$  and refractive index  $n_2$ , embedded in an infinite medium with refractive index  $n_1$ . In the cases considered in this work, both media have a relative magnetic permeability of unity.

Electromagnetic plane waves with angular frequency  $\omega$ , incident normally on the plate from the left or right, are given by  $A_{\text{in}} \exp\{i[\omega n_1(x - x_A)/c - \omega t]\}$  and  $B_{\text{in}} \exp\{i[-\omega n_1(x - x_B)/c - \omega t]\}$ , respectively, where  $c$  is the speed of light in vacuum and  $x_A$  ( $x_B$ ) is a point on the left (right) surface of the plate. The corresponding outgoing waves have the forms  $A_{\text{out}} \exp\{i[-\omega n_1(x - x_A)/c - \omega t]\}$  and  $B_{\text{out}} \exp\{i[\omega n_1(x - x_B)/c - \omega t]\}$ . Their amplitudes are related to those of the incident waves through a  $2 \times 2$  scattering matrix (the  $S$ -matrix) as follows

$$\begin{pmatrix} A_{\text{out}} \\ B_{\text{out}} \end{pmatrix} = \begin{pmatrix} r & t \\ t & r \end{pmatrix} \begin{pmatrix} A_{\text{in}} \\ B_{\text{in}} \end{pmatrix}, \quad (1)$$

with (see, e.g., Ref. [36])

$$r = \frac{(Z_1^2 - Z_2^2)[e^{2i\omega n_2 L/c} - 1]}{(Z_1 + Z_2)^2 - (Z_1 - Z_2)^2 e^{2i\omega n_2 L/c}} \quad (2)$$

and

$$t = \frac{4Z_1 Z_2 e^{i\omega n_2 L/c}}{(Z_1 + Z_2)^2 - (Z_1 - Z_2)^2 e^{2i\omega n_2 L/c}}. \quad (3)$$

We note that, while the standard definition of the scattering  $S$ -matrix refers all incoming and outgoing waves to a common origin [37], in our case, it is more convenient to expand the waves on the left and right sides of the plate using different reference points on the corresponding plate surfaces.

Setting  $\xi \equiv (Z_1 + Z_2)/(Z_1 - Z_2)$ , the eigenvalues of the  $S$ -matrix take the form

$$s_{1,2} = r \mp t = \mp \frac{\xi e^{i\omega n_2 L/c} \pm 1}{\xi \pm e^{i\omega n_2 L/c}} \quad (4)$$

with the associated eigenvectors being  $\mathbf{v}_{1,2} = (1 \mp 1)^T$ . It can be readily deduced from Eq. (4) that  $s_1$  has simple poles in the lower complex-frequency half-plane and corresponding zeros in the upper half-plane, situated symmetrically with respect to the real axis, specifically at

$$z_\nu^\mp \equiv (\omega + i\gamma)_\nu^\mp n_2 L/c = (2\nu + 1)\pi \mp i \ln \xi, \quad \nu \in \mathbb{Z}, \quad (5)$$

where the poles and the zeros are given by the “−” and “+” signs, respectively. Similarly, the poles and zeros of  $s_2$  appear at

$$z_\nu^\mp \equiv (\omega + i\gamma)_\nu^\mp n_2 L/c = 2\nu\pi \mp i \ln \xi, \quad \nu \in \mathbb{Z}. \quad (6)$$

The real parts of the frequencies given by Eqs. (5) and (6) correspond to the Fabry-Pérot resonance frequencies of the plate. That is, the poles and zeros of  $s_1$  ( $s_2$ ) yield the standing wave condition for plate thickness equal to odd (even) multiples of half-wavelength. It is also straightforward to show from Eq. (4) that the analytic continuation of the  $S$ -matrix in the complex frequency plane satisfies the general symmetry properties  $S(-z) = S^{-1}(z)$  and  $S(-z^*) = S^*(z)$  [38,39]. Figure 2 presents a plot of the modulus of the eigenvalues of the  $S$ -matrix in the complex frequency plane for a lossless dielectric plate of thickness  $L$  and refractive index  $n_2 = 3$ , embedded in an infinite medium with  $n_1 = 1$ , with both media having a relative magnetic permeability equal to unity.

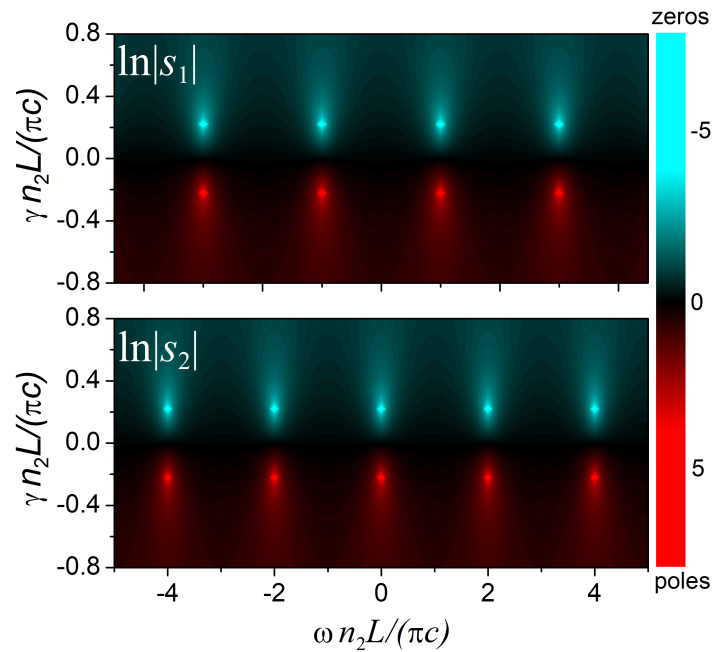


**Fig. 2.** Modulus (in logarithmic scale) of the eigenvalues of the  $S$ -matrix, as described by Eq. (4), for a lossless dielectric plate of thickness  $L$  and refractive index  $n_2 = 3$ , embedded in an infinite medium with  $n_1 = 1$ , in the complex-frequency plane. The relative magnetic permeability of both media is equal to unity. The positions of the zeros and poles, given by Eq. (6), are indicated by the bright cyan and red points, respectively.

### 3. Coherent virtual absorption

#### 3.1. Transient response to abrupt excitation cutoff

We assume an electromagnetic field of complex frequency  $\omega + i\gamma$ , where  $\gamma > 0$ , incident on a plate from both sides. At points  $x_A$  and  $x_B$  on the plate surfaces, this field is given by

$$E_{\text{in}}(t) = e^{-i\omega t} e^{\gamma t} \Theta(-t), \quad (7)$$

where the Heaviside step function,  $\Theta(-t)$ , enforces an instantaneous cutoff at  $t = 0$ , to prevent the incoming wave's amplitude from growing indefinitely as  $t \rightarrow \infty$ .

The field given by Eq. (7) can be expanded into real-frequency waves using the Fourier transform, following the  $E \sim \exp(-i\omega t)$  convention, as follows

$$E_{\text{in}}(t) = \frac{1}{2\pi} \int_{-\infty}^{\infty} d\omega' \tilde{E}(\omega') e^{-i\omega' t},$$

where  $\tilde{E}(\omega') = \int_{-\infty}^{\infty} dt' E_{\text{in}}(t') e^{i\omega' t'} = \frac{-i}{\omega' - \omega - i\gamma}$ . Thus,  $E_{\text{in}}(t)$  takes the form

$$E_{\text{in}}(t) = \frac{1}{2\pi i} \int_{-\infty}^{\infty} d\omega' \frac{1}{\omega' - \omega - i\gamma} e^{-i\omega' t}. \quad (8)$$

We now calculate the outgoing field at the left and right edges of the plate, choosing the incident complex frequency  $(\omega + i\gamma)n_2L/c \equiv z$  to be exactly at a zero,  $z_p^+$ , of  $s_2$ , given by Eq. (6) for  $\nu = p$ . Since  $s_2$  corresponds to the eigenvector  $\mathbf{v}_2 = (1 \ 1)^T$ , the incoming waves are identical on both sides of the plate, and so are the outgoing waves. From Eqs. (1) and (8), setting  $\tau \equiv ct/(n_2L)$ , the outgoing field  $E_{\text{out}}$  takes the form

$$E_{\text{out}}(\tau) = \frac{1}{2\pi i} \int_{-\infty}^{\infty} dz' \frac{s_2(z')}{z' - z_p^+} e^{-iz'\tau}. \quad (9)$$

This integral can be analytically evaluated in the complex plane using Jordan's lemma in conjunction with the residue theorem [40].

For  $\tau < 0$ , by Jordan's lemma, we close the integration path of Eq. (9) with a semicircular contour  $C_R = \{Re^{i\theta} | \theta \in [0, \pi]\}$  of radius  $R \rightarrow \infty$  in the upper complex half-plane. From Eq. (6) (see also Fig. 2) it is evident that all poles of  $s_2$  are located in the lower complex half-plane. Thus, the only pole inside the integration path is at  $z_p^+$ , leading to

$$E_{\text{out}}(\tau) = \frac{1}{2\pi i} (2\pi i) s_2(z_p^+) e^{-iz_p^+ \tau} = 0, \quad \tau < 0. \quad (10)$$

As expected, selecting the incident complex frequency at a zero of  $s_2$  is the key to achieving coherent perfect absorption. Since  $E_{\text{out}} = 0$  for  $\tau < 0$ , all incident radiation remains stored within the plate during illumination.

For  $\tau > 0$ , by Jordan's lemma, the integration path of Eq. (9) can be closed with a semicircular contour of infinite radius in the lower complex half-plane, enclosing the simple poles of  $s_2(z) = [\xi \exp(iz) - 1]/[\xi - \exp(iz)]$  at  $z = z_v^-$ . Using Eq. (6) and the relation  $\exp(iz_v^-) = \xi$ , the residue at each pole takes the form

$$\begin{aligned} R_\nu &= \frac{1}{z_v^- - z_p^+} \frac{\xi e^{iz_v^-} - 1}{-ie^{iz_v^-}} e^{-iz_v^- \tau} \\ &= \frac{-1}{2\pi(\nu - p) - 2i \ln \xi} \frac{\xi^2 - 1}{i\xi} e^{-2\pi i \nu \tau} e^{-(\ln \xi)\tau}. \end{aligned}$$

From residue theorem, setting  $n \equiv p - \nu$ , we obtain

$$\begin{aligned}
 E_{\text{out}}(\tau) &= \frac{1}{2\pi i} (-2\pi i) \sum_{\nu=-\infty}^{\infty} R_{\nu} \\
 &= -i \frac{\xi^2 - 1}{2\pi\xi} e^{-2\pi i p \tau} e^{-(\ln \xi)\tau} \sum_{n=-\infty}^{\infty} \frac{e^{2\pi i n \tau}}{\frac{-i \ln \xi}{\pi} - n}.
 \end{aligned} \tag{11}$$

It can be shown (see Appendix) that the infinite series  $\sum_{n=-\infty}^{\infty} \exp(2\pi i n \tau)/(z - n)$ , with  $z \in \mathbb{C} \setminus \mathbb{Z}$ , represents the Fourier expansion of  $2\pi i f(\tau)$ , where  $f(\tau)$  is a periodic piecewise continuous function on  $[0, 1]$  given by  $\exp(2\pi i z \tau)/[\exp(2\pi i z) - 1]$ . This relationship also results from the properties of the Hurwitz-Lerch zeta function, although under the more restrictive condition that  $|z| < 1$  [41]. Using this identity, Eq. (11) for  $\tau > 0$  yields  $E_{\text{out}}(\tau) = e^{-2\pi i p \tau} \xi^{(\tau-1-2\lfloor \tau \rfloor)}$ , where  $\lfloor \tau \rfloor$  denotes the integer part of  $\tau$ . Therefore, for incident waves described by Eq. (7) with  $\omega n_2 L/c = 2p\pi$ ,  $p \in \mathbb{Z}$ , and  $\gamma n_2 L/c = \ln \xi$ , the outgoing waves are given by the closed-form expression

$$E_{\text{out}}(\tau) = e^{-2\pi i p \tau} \xi^{\tau-1-2\lfloor \tau \rfloor} \Theta(\tau). \tag{12}$$

Figure 3 illustrates the time variation of the electric field for the incoming and outgoing radiation at points  $x_A$  and  $x_B$  on the surfaces of a plate of thickness  $L$  and refractive index  $n_2 = 3$  embedded in a medium with  $n_1 = 1$  (we assume that both media have a relative magnetic permeability equal to unity), as given by Eqs. (7) and (12), respectively. The discontinuities of  $E_{\text{out}}(\tau)$  that occur at  $\tau \in \mathbb{N}$ :  $\lim_{\epsilon \rightarrow 0} [E_{\text{out}}(\tau + \epsilon) - E_{\text{out}}(\tau - \epsilon)] = \xi^{-\tau-1} - \xi^{-\tau+1}$  for  $\tau \in \mathbb{N}$  arise from the instantaneous interruption of the excitation. In fact, this unnatural discontinuity of  $E_{\text{in}}(\tau)$  at  $\tau = 0$  is conveyed to the outgoing waves, appearing at integer multiples of the time  $t = n_2 L/c$ , i.e.  $\tau = 1$ , which is the time it takes for the wave to travel between the two edges of the plate. In the case of continuous excitation,  $E_{\text{out}}$  is also continuous (see Subsection 3.2). It is worth noting that, as implied by Eqs. (7) and (12) and illustrated in Fig. 3, the outgoing field at time  $\tau$  is equal to the incident field at  $\tau - 1 - 2\lfloor \tau \rfloor$ . In the bottom diagram of Fig. 3 we present the electromagnetic energy inside the plate as a function of time, which is proportional to  $\int dt \{\text{Re}[E(t)]\}^2$ . For the duration of illumination,  $t < 0$ , all incoming radiation is stored in the plate since  $E_{\text{out}} = 0$ . In the absence of losses, when the incident field is abruptly interrupted at  $t = 0$ , the plate starts to emit radiation in distinct packets until all stored energy is completely depleted.

### 3.2. Transient response to smoothed excitation cutoff

In order to study a more realistic excitation, let us consider an incident field of complex frequency  $\omega + i\gamma$ ,  $\gamma > 0$ , that starts to decay at  $t = 0$  at an exponential rate of  $\Gamma \equiv \alpha\gamma$ ,  $\alpha \in \mathbb{R} \setminus \{1\}$ . At points  $x_A$  and  $x_B$  on the surfaces of the plate, this field has the form

$$E_{\text{in}}(t) = e^{-i\omega t} e^{\gamma t} \Theta(-t) + e^{-i\omega t} e^{-\Gamma t} \Theta(t). \tag{13}$$

By applying a Fourier transform we obtain

$$E_{\text{in}}(t) = \frac{1}{2\pi i} \int_{-\infty}^{\infty} d\omega' \left[ \frac{1}{\omega' - \omega - i\gamma} - \frac{1}{\omega' - \omega + i\Gamma} \right] e^{-i\omega' t}. \tag{14}$$

Following the same steps taken after Eq. (8), the outgoing field is written as

$$\begin{aligned}
 E_{\text{out}}(\tau) &= \frac{1}{2\pi i} \int_{-\infty}^{\infty} dz' \frac{s_2(z')}{z' - z_p^+} e^{-iz'\tau} \\
 &\quad - \frac{1}{2\pi i} \int_{-\infty}^{\infty} dz' \frac{s_2(z')}{z' - z_{\Gamma}} e^{-iz'\tau} \equiv E_{\text{out}}^{\text{I}}(\tau) + E_{\text{out}}^{\text{II}}(\tau),
 \end{aligned} \tag{15}$$

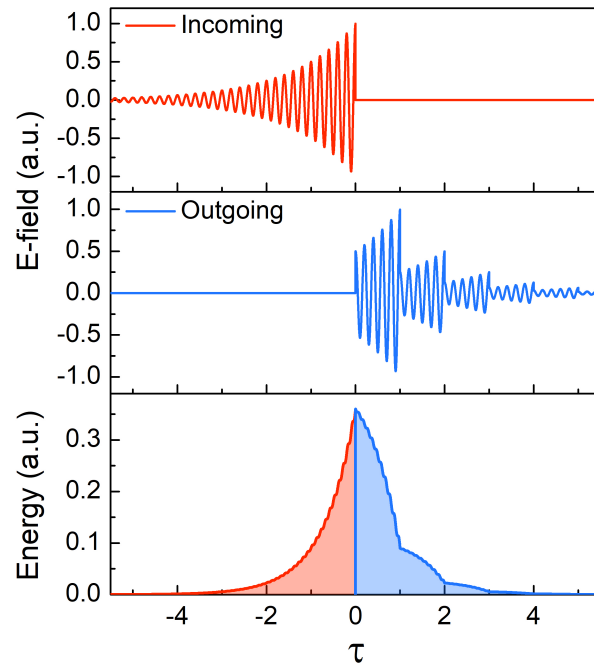


**Fig. 3.** Upper diagrams: Time evolution of the real-valued electric field (in arbitrary units) observed at points  $x_A$  and  $x_B$  on the surfaces of a plate with thickness  $L$  and refractive index  $n_2 = 3$ , embedded in a medium with  $n_1 = 1$  (both media have a relative magnetic permeability equal to unity), upon a complex-frequency excitation given by Eq. (7) with  $\omega n_2 L/c = 10\pi$  and  $\gamma n_2 L/c = \ln \xi$ . Bottom diagram: Corresponding variation of the electromagnetic energy inside the plate (in arbitrary units).

where  $z_\Gamma \equiv (\omega - i\Gamma)n_2 L/c = 2p\pi - i\alpha \ln \xi$ . The first integral,  $E_{\text{out}}^I(\tau)$ , is the same as in Eq. (9) and will obviously lead to the result of Eq. (12). The poles of the integrand of the second integral, which yields  $E_{\text{out}}^{II}(\tau)$ , are those of  $s_2$  given by Eq. (4), plus the simple pole at  $z = z_\Gamma$ , which is also in the lower complex half-plane.

From Jordan's lemma, for  $\tau < 0$ , the integration path can be closed with a semicircular contour of infinite radius in the upper half-plane, and the residue theorem yields  $E_{\text{out}}(\tau) = E_{\text{out}}^I(\tau) + E_{\text{out}}^{II}(\tau) = 0$ , since  $E_{\text{out}}^I(\tau) = 0$  from Eq. (10) and the integrand that produces  $E_{\text{out}}^{II}(\tau)$  has no poles in the upper complex half-plane.

Regarding  $E_{\text{out}}^{II}(\tau)$  when  $\tau > 0$ , by Jordan's lemma the integration path can be closed with a semicircular contour of infinite radius in the lower half-plane and the residues at the poles  $z_\Gamma$  and  $z_\nu^-$  involved take the form

$$R_\Gamma = \frac{\xi e^{iz_\Gamma} - 1}{\xi - e^{iz_\Gamma}} e^{-iz_\Gamma \tau} \text{ and } R_\nu = \frac{1}{z_\nu^- - z_\Gamma} \frac{\xi^2 - 1}{-i\xi} e^{-iz_\nu^- \tau},$$

respectively. Then, by applying the residue theorem we obtain

$$\begin{aligned} E_{\text{out}}^{II}(\tau) &= -\frac{1}{2\pi i} (-2\pi i) R_\Gamma - \frac{1}{2\pi i} (-2\pi i) \sum_{\nu=-\infty}^{\infty} R_\nu \\ &= R_\Gamma + i \frac{\xi^2 - 1}{2\pi \xi} e^{-(\ln \xi)\tau} \sum_{\nu=-\infty}^{\infty} \frac{e^{2\pi i \nu \tau}}{\frac{-z_\Gamma - i \ln \xi}{2\pi} - \nu}. \end{aligned} \tag{16}$$

The infinite series in Eq. (16) is essentially identical to the one in Eq. (11) and can be handled in the same way. Consequently, after some straightforward algebra, the scattered field takes its final form

$$E_{\text{out}}(\tau) = e^{-2\pi i p \tau} \left[ \xi^{\tau-1-2|\tau|} - \xi^{-\alpha\tau-1} \frac{\xi^{\alpha+1} - 1}{\xi^{\alpha-1} - 1} - (\xi^2 - 1) \frac{\xi^{-\alpha(\tau-|\tau|)-|\tau|-1}}{\xi^{1-\alpha} - 1} \right] \Theta(\tau). \quad (17)$$

We recall that  $\omega n_2 L/c = 2p\pi$ ,  $p \in \mathbb{Z}$ ,  $\gamma n_2 L/c = \ln \xi$  and  $\Gamma = \alpha\gamma$  with  $\alpha \in \mathbb{R} \setminus \{1\}$ . For  $\alpha = 1$ , the pole at  $z_\Gamma$  coincides with one of the poles of  $s_2(z)$ , resulting in a second-order pole that requires separate and distinct treatment in the residue calculation [40].

Interestingly, unlike the outgoing field in Eq. (12), which exhibits discontinuities at  $\tau \in \mathbb{N}$ , the field in Eq. (17) remains continuous due to the smooth nature of the excitation. In fact, it is straightforward to show that, in this case,  $\lim_{\epsilon \rightarrow 0} [E_{\text{out}}(\tau + \epsilon) - E_{\text{out}}(\tau - \epsilon)] = 0$  for  $\tau \in \mathbb{N}$ . It is also worth noting that, in the limit  $\alpha \rightarrow \infty$ , corresponding to an abrupt cutoff of the excitation, we recover Eq. (12). Moreover, for  $\alpha = -1$ , which represents an excitation that grows exponentially without bound as time evolves, the outgoing field vanishes identically.

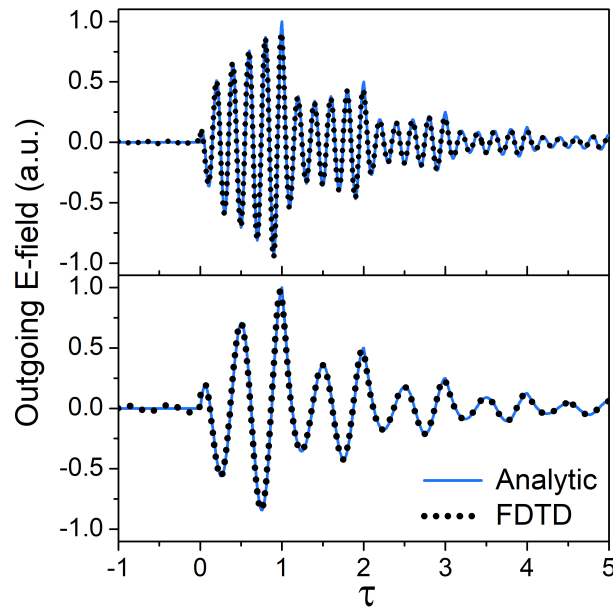


**Fig. 4.** Time evolution of the real-valued outgoing electric field (in arbitrary units) observed at points  $x_A$  and  $x_B$  on the surfaces of a plate with thickness  $L$  and refractive index  $n_2 = 3$ , embedded in a medium with  $n_1 = 1$  (both media have a relative magnetic permeability equal to unity), upon a complex-frequency excitation given by Eq. (13) with  $\gamma n_2 L/c = \ln \xi$ ,  $\Gamma = 15\gamma$ ,  $\omega n_2 L/c = 10\pi$  (top) and  $\omega n_2 L/c = 4\pi$  (bottom). The analytical solution of Eq. (17) is depicted by solid lines, while the finite-difference-time-domain (FDTD) simulations, are represented by dotted lines.

Figure 4 shows the time variation of the outgoing fields, given by Eq. (17), in the same system as in Fig. 3, for an excitation defined by Eq. (13) with  $\gamma n_2 L/c = \ln \xi$ ,  $\Gamma = 15\gamma$ ,  $\omega n_2 L/c = 10\pi$  (top plot) and  $\omega n_2 L/c = 4\pi$  (bottom plot). When comparing Fig. 4 with Fig. 3, it is evident that the discontinuities of  $E_{\text{out}}$  are no longer present. However, the envelope function in Eq. (17) still leads to outgoing waves appearing in distinct packets, each with a duration of  $t = n_2 L/c$ , i.e.  $\tau = 1$ , as can be clearly seen in the upper plot of Fig. 4. Moreover, smoothing the excitation for  $\tau > 0$  facilitates finite-difference simulations by removing discontinuities. Figure 4 presents the

analytical solutions alongside the corresponding simulations, demonstrating excellent agreement for the two different values of  $\omega$  considered. The upper plot depicts the outgoing field for  $\omega n_2 L/c = 10\pi$ , providing a comparison with the abrupt excitation cutoff shown in Fig. 3. The bottom plot, with  $\omega n_2 L/c = 4\pi$  and the previously mentioned choice of  $\Gamma = 15\gamma$ , was designed to approximate the excitation employed by Baranov *et al.* [3], who used a Gaussian decay, yielding very similar results for the outgoing fields.

#### 4. Conclusion

In summary, we presented a comprehensive analysis of the effect of coherent virtual absorption in a lossless dielectric plate. Starting with the Fourier transform of the excitation function, we applied complex integration techniques, including Jordan's lemma and the residue theorem, to analytically derive exact closed-form expressions for the transient response of the plate under complex-frequency excitation. This derivation fully accounts for the analytic structure of the scattering  $S$ -matrix in the complex-frequency plane, ensuring a rigorous characterization of the system's behavior. The application of the residue theorem leads to infinite series, the summation of which presents a key challenge in the derivation but is successfully addressed within the analytical framework, resulting in formulas that show excellent agreement with numerical simulations and provide deep physical insight into the underlying mechanisms.

Furthermore, our rigorous theoretical analysis not only confirms earlier observations, but also uncovers several intriguing phenomena that had been previously overlooked. Notably, we identify discontinuities in the outgoing scattered field and reveal that the stored energy is released in distinct packets. These findings offer a deeper understanding of the transient dynamics of the system and may inspire further investigations.

Beyond the specific case of a lossless dielectric plate, our analytical approach is highly versatile and can be applied to various scattering structures and physical systems, offering a robust framework for further theoretical and experimental research in this field.

#### Appendix

Let us consider the function

$$f(\tau) = \frac{e^{2\pi iz\tau}}{e^{2\pi iz} - 1}, \quad (18)$$

where  $z \in \mathbb{C} \setminus \mathbb{Z}$ , defined for  $0 < \tau < 1$ , and satisfying the periodicity condition  $f(\tau + 1) = f(\tau)$ . This function exhibits discontinuities of first kind for integer values of  $\tau$ . The Fourier series expansion of  $f(\tau)$  is given by

$$f(\tau) = \sum_{n=-\infty}^{\infty} \tilde{f}_n e^{2\pi in\tau}, \quad (19)$$

where  $\tilde{f}_n = \int_0^1 d\tau e^{-2\pi in\tau} f(\tau) = \frac{1}{2\pi i(z - n)}$ . Therefore,

$$2\pi if(\tau) = \sum_{n=-\infty}^{\infty} \frac{e^{2\pi in\tau}}{z - n}, \quad z \in \mathbb{C} \setminus \mathbb{Z}. \quad (20)$$

**Funding.** Hellenic Foundation for Research and Innovation (4509, 16909); General Secretariat for Research and Innovation.

**Disclosures.** The authors declare no conflicts of interest.

**Data availability.** Data underlying the results presented in this paper are not publicly available at this time but may be obtained from the authors upon reasonable request.

## References

1. K. C. Huang, E. Lidorikis, X. Jiang, *et al.*, “Nature of lossy bloch states in polaritonic photonic crystals,” *Phys. Rev. B* **69**(19), 195111 (2004).
2. K. L. Tsakmakidis, T. W. Pickering, J. M. Hamm, *et al.*, “Completely stopped and dispersionless light in plasmonic waveguides,” *Phys. Rev. Lett.* **112**(16), 167401 (2014).
3. D. G. Baranov, A. Krasnok, and A. Alù, “Coherent virtual absorption based on complex zero excitation for ideal light capturing,” *Optica* **4**(12), 1457–1461 (2017).
4. F. Guan, X. Guo, K. Zeng, *et al.*, “Overcoming losses in superlenses with synthetic waves of complex frequency,” *Science* **381**(6659), 766–771 (2023).
5. S. Kim, Y.-G. Peng, S. Yves, *et al.*, “Loss compensation and superresolution in metamaterials with excitations at complex frequencies,” *Phys. Rev. X* **13**(4), 041024 (2023).
6. F. Guan, X. Guo, S. Zhang, *et al.*, “Compensating losses in polariton propagation with synthesized complex frequency excitation,” *Nat. Mater.* **23**(4), 506–511 (2024).
7. S. Longhi, “Coherent virtual absorption for discretized light,” *Opt. Lett.* **43**(9), 2122–2125 (2018).
8. G. Trainiti, Y. Ra’di, M. Ruzzene, *et al.*, “Coherent virtual absorption of elastodynamic waves,” *Sci. Adv.* **5**(8), eaaw3255 (2019).
9. Q. Zhong, L. Simonson, T. Kottos, *et al.*, “Coherent virtual absorption of light in microring resonators,” *Phys. Rev. Res.* **2**(1), 013362 (2020).
10. A. Marini, D. Ramaccia, A. Toscano, *et al.*, “Metasurface-bounded open cavities supporting virtual absorption: free-space energy accumulation in lossless systems,” *Opt. Lett.* **45**(11), 3147–3150 (2020).
11. A. V. Marini, D. Ramaccia, A. Toscano, *et al.*, “Metasurface virtual absorbers: unveiling operative conditions through equivalent lumped circuit model,” *EPJ Appl. Metamat.* **8**(3), 3 (2021).
12. A. V. Marini, D. Ramaccia, A. Toscano, *et al.*, “Perfect matching of reactive loads through complex frequencies: From circuit analysis to experiments,” *IEEE Trans. Antennas Propag.* **70**(10), 9641–9651 (2022).
13. A. Farhi, A. Mekawy, A. Alù, *et al.*, “Excitation of absorbing exceptional points in the time domain,” *Phys. Rev. A* **106**(3), L031503 (2022).
14. T. Delage, J. Sokoloff, O. Pascal, *et al.*, “Plasma ignition via high-power virtual perfect absorption,” *ACS Photonics* **10**(10), 3781–3788 (2023).
15. D. V. Novitsky and A. S. Shalin, “Virtual perfect absorption in resonant media and their  $\mathcal{PT}$ -symmetric generalizations,” *Phys. Rev. A* **108**(5), 053513 (2023).
16. Y. Ra’di, A. Krasnok, and A. Alù, “Virtual critical coupling,” *ACS Photonics* **7**(6), 1468–1475 (2020).
17. T. Delage, O. Pascal, J. Sokoloff, *et al.*, “Experimental demonstration of virtual critical coupling to a single-mode microwave cavity,” *J. Appl. Phys.* **132**(15), 153105 (2022).
18. S. Lepeshov and A. Krasnok, “Virtual optical pulling force,” *Optica* **7**(8), 1024–1030 (2020).
19. H. Li, A. Mekawy, A. Krasnok, *et al.*, “Virtual parity-time symmetry,” *Phys. Rev. Lett.* **124**(19), 193901 (2020).
20. Z. Chen, H. He, H. Li, *et al.*, “Observation of parity-time symmetry for evanescent waves,” *Commun. Phys.* **7**(1), 339 (2024).
21. R. Ali, “Lighting of a monochromatic scatterer with virtual gain,” *Phys. Scr.* **96**(9), 095501 (2021).
22. A. M. B. Bradley, W. Tuxbury, and T. Kottos, “Directed emission from uniformly excited non-hermitian photonic meta-structures,” *Opt. Lett.* **47**(22), 5913–5916 (2022).
23. Z. Gu, H. Gao, H. Xue, *et al.*, “Transient non-hermitian skin effect,” *Nat. Commun.* **13**(1), 7668 (2022).
24. S. Kim, S. Lepeshov, A. Krasnok, *et al.*, “Beyond bounds on light scattering with complex frequency excitations,” *Phys. Rev. Lett.* **129**(20), 203601 (2022).
25. C. Rasmussen, M. I. N. Rosa, J. Lewton, *et al.*, “A lossless sink based on complex frequency excitations,” *Adv. Sci.* **10**(28), 2301811 (2023).
26. D. V. Novitsky, “Tunable virtual gain in resonantly absorbing media,” *Phys. Rev. A* **107**(1), 013516 (2023).
27. R. Ali, T. P. M. Alegre, and G. S. Wiederhecker, “Enhancing the goos-hänchen and spin-hall shifts in planar and spherical structures through complex-frequency excitations,” *Phys. Rev. B* **110**(8), 085403 (2024).
28. G. P. Zouros, I. Loulas, E. Almpanis, *et al.*, “Anisotropic virtual gain and large tuning of particles’ scattering by complex-frequency excitations,” *Commun. Phys.* **7**(1), 283 (2024).
29. J. Hinney, S. Kim, G. J. K. Flatt, *et al.*, “Efficient excitation and control of integrated photonic circuits with virtual critical coupling,” *Nat. Commun.* **15**(1), 2741 (2024).
30. H. Gao, W. Zhu, H. Xue, *et al.*, “Controlling acoustic non-hermitian skin effect via synthetic magnetic fields,” *Appl. Phys. Rev.* **11**(3), 031410 (2024).
31. T. Jiang, C. Zhang, R.-Y. Zhang, *et al.*, “Observation of non-hermitian boundary induced hybrid skin-topological effect excited by synthetic complex frequencies,” *Nat. Commun.* **15**(1), 10863 (2024).
32. K. Zeng, C. Wu, X. Guo, *et al.*, “Synthesized complex-frequency excitation for ultrasensitive molecular sensing,” *eLight* **4**(1), 1 (2024).
33. X. Zhu, D. Liao, P. Tang, *et al.*, “Decoupled dipole arrays empowered by invisible complex poles in epsilon-near-zero metamaterials,” *Adv. Funct. Mater.* **35**(1), 2412057 (2025).
34. J.-X. Zhong, P. F. de Castro, T. Lu, *et al.*, “Higher-order skin effect and its observation in an acoustic kagome lattice,” *Phys. Rev. B* **111**(1), 014314 (2025).

35. F. Guan, Y. Yang, H.-C. Chan, *et al.*, “Excitation of longitudinal bound states in a weyl metamaterial cavity,” *Laser & Photonics Reviews* **19**(8), 2400914 (2025).
36. M. Born and E. Wolf, *Principles of Optics: Electromagnetic Theory of Propagation, Interference and Diffraction of Light* (Cambridge University, 1999), 7th ed.
37. G. Gantzounis and N. Stefanou, “Layer-multiple-scattering method for photonic crystals of nonspherical particles,” *Phys. Rev. B* **73**(3), 035115 (2006).
38. N. G. van Kampen, “*s*-matrix and causality condition. i. maxwell field,” *Phys. Rev.* **89**(5), 1072–1079 (1953).
39. N. G. van Kampen, “The symmetry relation of the *s* matrix in the complex plane,” *Physica* **20**(1-6), 115–123 (1954).
40. M. J. Ablowitz and A. S. Fokas, “Complex Variables: Introduction and Applications,” *Cambridge Texts in Applied Mathematics* (Cambridge University, 2003), 2nd ed.
41. S. Kanemitsu, M. Katsurada, and M. Yoshimoto, “On the Hurwitz—Lerch zeta-function,” *Aequ. math.* **59**(1), 1–19 (2000).